19. Tensile failure and spalling

Introduction

The purpose of this chapter is to summarize the combinations of in situ stress and rock properties that can lead to tensile failure, spalling and one type of rockbursting of intact or sparsely jointed, massive rock surrounding tunnels and boreholes. Generally, tensile failure occurs at much lower stress levels than spalling. It occurs first and progresses until the cracks have reached a stable configuration. As the stress levels increase, spalling can be initiated. This also progresses in a stepwise manner until a stable configuration is reached and the spalls stop. At much higher stress levels, cracks remote from the excavation boundary can interact with the tensile cracks and spalls to create a large-scale shear fracture. This can collapse the tunnel with the release of a significant amount of energy which may be one of the mechanisms responsible for the violent failures known as rockbursts.

Numerous papers on each, or on all these failure mechanisms, have been published. Several of these will be referred to in this chapter. While the general conclusions reached are similar, a wide range of different opinions on details of the failure mechanisms have been published. In the discussion which follows, a set of mechanisms will be presented which appear to fit numerous practical observations that I have made over the years. I make no claim that these mechanisms are more logical or correct than alternative mechanisms proposed, but they do provide credible explanations for understanding these failure processes.

Failure initiation and propagation in intact rock surrounding a tunnel

Figure 1 illustrates the in-situ and the induced stresses around the boundary of a circular excavation such as a tunnel or borehole in intact or sparsely jointed massive rock. In this case, it has been assumed that the maximum principal stress P acts in a horizontal direction and that the minor principal stress kP has a much lower magnitude. If the value of $k < 0.33$, then tensile stress zones will be induced in the excavation sidewalls as illustrated.

When the tensile stresses on the boundary exceed the tensile strength of the rock, horizontal cracks will develop in the rock as illustrated in Figure 2. There may be several parallel cracks, with very small opening widths, as illustrated in the right-hand sidewall of the lower figure, or, there may be a single wider crack as shown in the left-hand sidewall. These tensile cracks propagate a limited distance before stopping and becoming completely stable. The development of spalling in the roof and floor of the circular excavation is illustrated in Figure 2. The distance to which single cracks will propagate was determined by Hoek (1965) in glass and rock plate models, as illustrated in Figures 3 and 4.

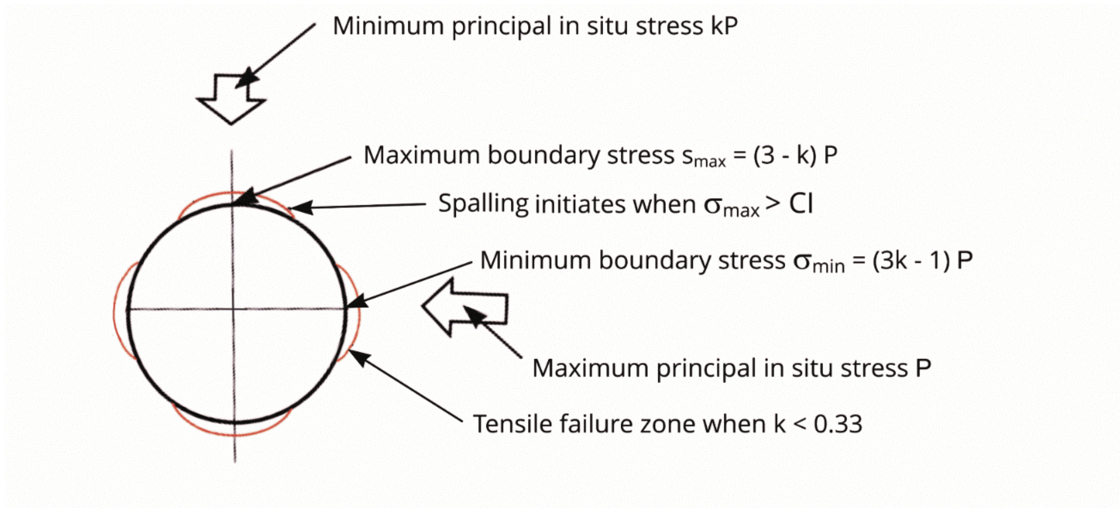

Figure 1: Stress conditions in a highly stressed intact or sparsely jointed massive rock surrounding a circular tunnel or borehole.

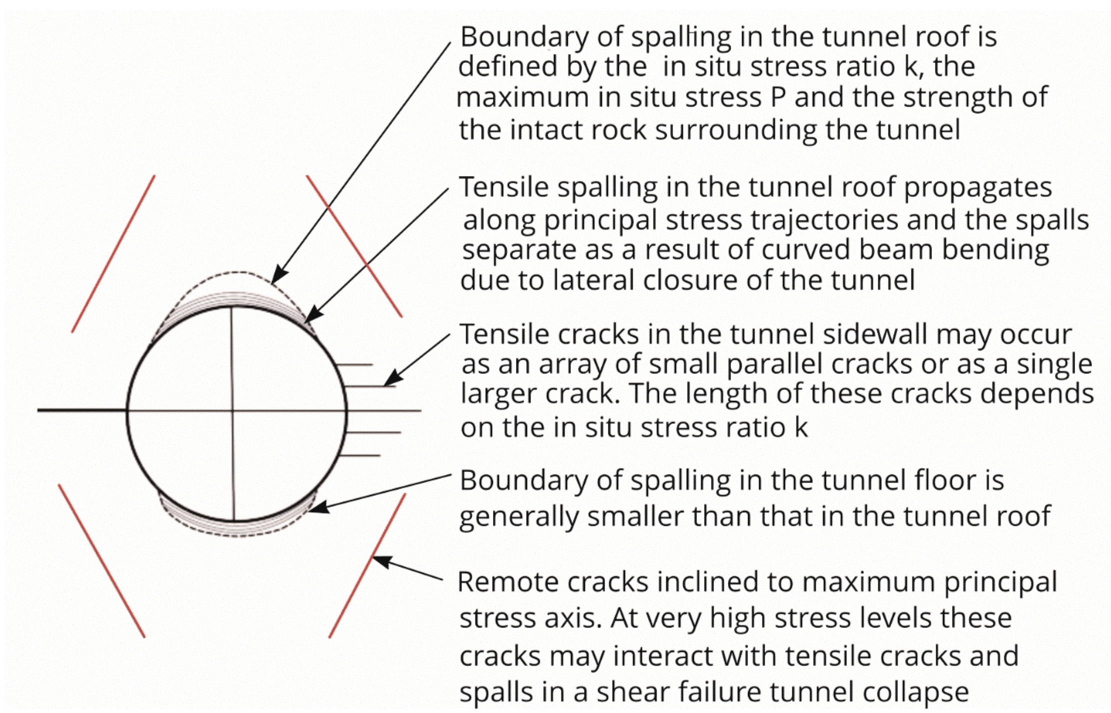

Figure 2: Failure types in a highly stressed intact or sparsely jointed massive rock surrounding a circular tunnel or borehole.

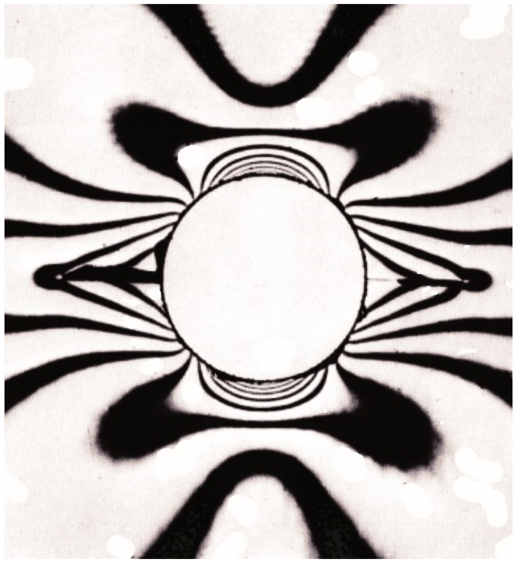

Figure 3: Photoelastic pattern in a glass plate model showing the distribution of $(\sigma_1 - \sigma_3)$ contours and the formation of tensile cracks in the sidewalls.

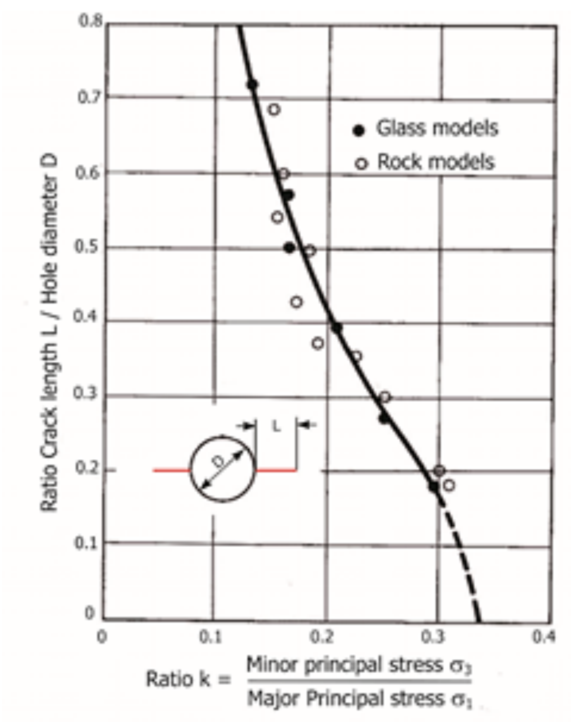

Figure 4: Length of stable cracks in glass and rock models tested by Hoek (1965).

Spalling initiates when the boundary stress exceeds the crack initiation stress CI in the roof and floor of the tunnel, as shown in Figure 1. Nicksair and Martin (2013) showed that tensile crack initiation (CI) in various rocks can initiate at approximately 45% of the uniaxial compressive strength (UCS) of the intact rock. This crack initiation is a pre-requisite for spalling. It is necessary to establish the in-situ stress conditions that can cause the initiation of these cracks when a tunnel is excavated in an intact or sparsely jointed rock mass.

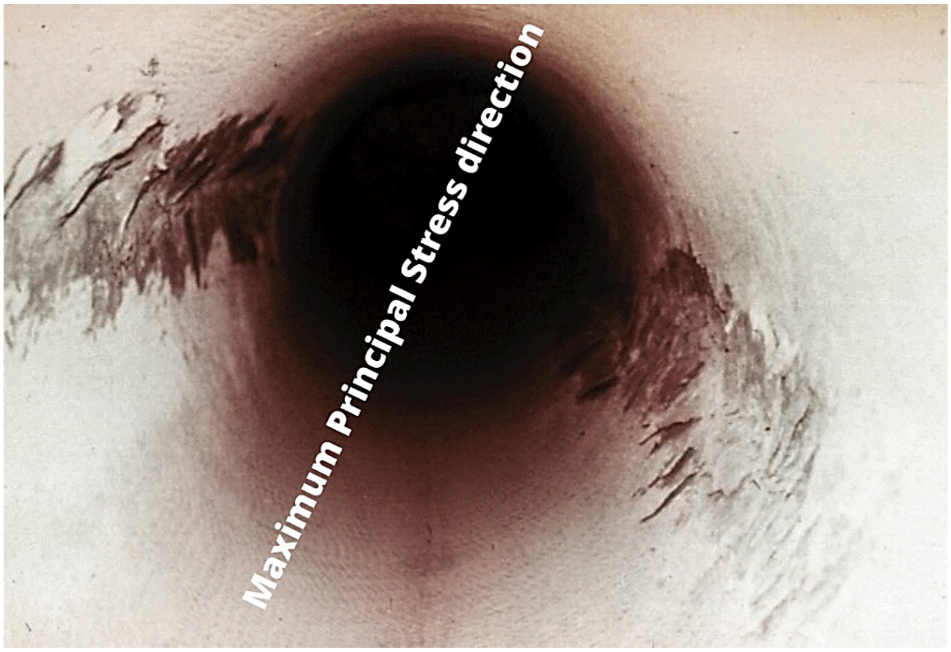

Figure 5: Spalling in the sidewalls of a machine bored mine shaft in massive rock.

A typical spall from the walls of a machine bored shaft or tunnel in highly stressed massive rock is illustrated in Figure 5. These spalls initiate on the tunnel boundary, at points of maximum compressive stress which are defined by the normal to the maximum principal stress direction. As shown in Figure 1, the maximum boundary stress at these locations is $\sigma_{1max} = (3 - k)\,P$, where k is the ratio of minor to major principal stresses (σ_3/σ_1) and P is the magnitude of the major in situ principal stress. As discussed above, spalling initiates when the maximum boundary stress exceeds the crack initiation strength CI. This results in the spalling initiation relationship:

$$CI = (3 - k)P \tag{1}$$

Observation of spalling in the field show that, in massive intact rock, the spalls occur as thin plates such as that illustrated in Figure 6. As shown in the close-up photograph reproduced in Figure 7, the appearance of the spall surface suggests that it has occurred because of pure tensile failure, with no signs of slickensides which are normally associated with shear failure. This, in turn, suggests that the spalling is controlled by tensile failure rather than by shearing, which is the default failure mode assumed in many numerical programs used for shaft and tunnel failure analysis.

Figure 6: Plate-like spall from a tunnel in massive granite.

Figure 7: Spalls showing tensile failure surfaces with no signs of slickensides associated with shearing.

Figure 8 shows the mechanism of spalling proposed by Dyskin and Germanovich (1993). This involves the propagation of wing cracks formed at the tips of existing microcracks in the rock, which, as shown by several authors in Figure 9, depends upon the reduction of the ratio of the minor to major principal stresses. As this ratio decreases close to zero at the excavation boundary, the wing crack length increases to the full extent of the overstressed section of the boundary and thin plates are formed. As shown in Figures 6 and 7, these plates are typically 1 to 2 cm thick in 4 to 5 m diameter tunnels.

As suggested in Figure 8, once a slender slab has developed in the wall of an excavation, any additional loading will apply an axial load to this plate. This will result in bending failure of the plate and a creation of a new excavation boundary behind which a new spall will initiate. The process tends to be self-propagating until conditions are reached which make it difficult or impossible for new spalls to develop.

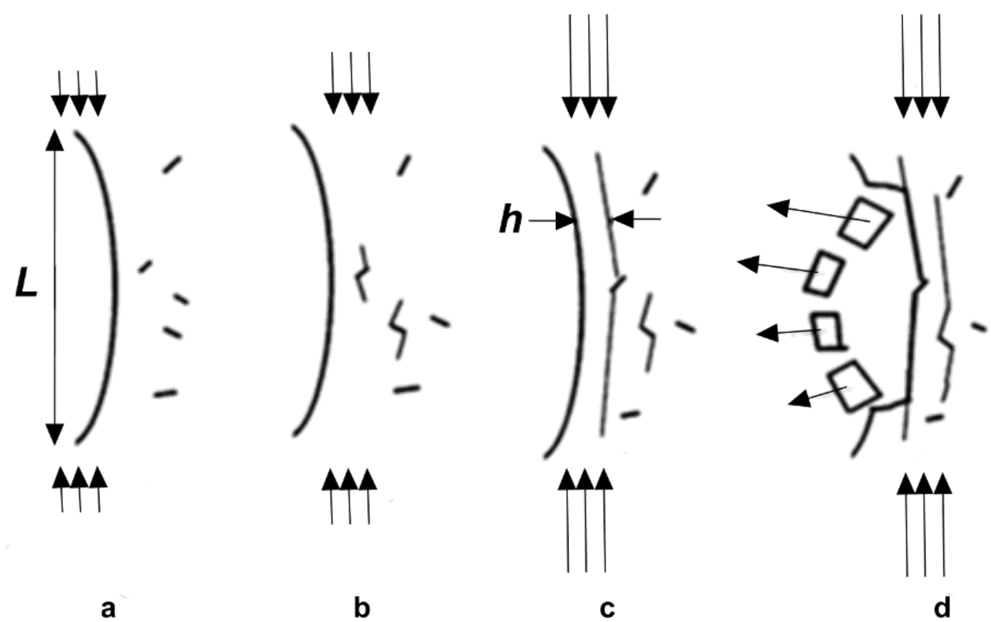

a. Existing microcracks in the rock adjacent to the excavation boundary
b. Propagation of wing cracks from isolated microcracks as stress increases
c. Propagation of wing cracks from microcrack close to excavation boundary due to lack of confinement
d. Buckling failure of spall adjacent to excavation boundary and creation of a new spall due to lateral stress relief

Figure 8: Simplified illustration of the mechanism of spall formation, from Dyskin and Germanovich, 1993.

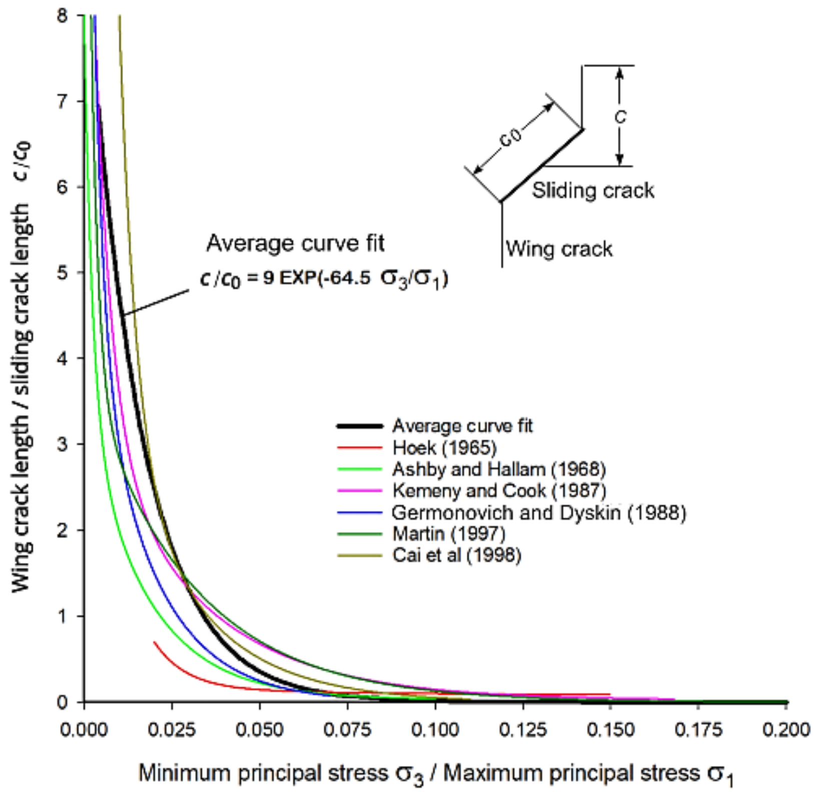

Figure 9: Vertical wing crack length from critically inclined Griffith cracks for different ratios of minor to major principal stress.

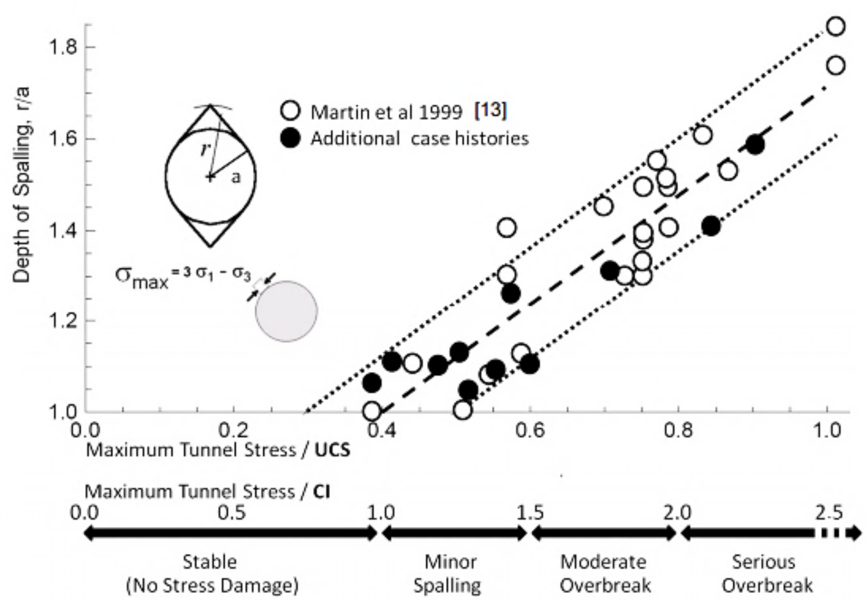

Figure 10: Plot of measured depth of spalling for a circular tunnel by Diederichs et al. (2010).

The most important of these conditions is the overall shape of the complete set of spalls in relation to the ratio of the maximum stress in the tunnel wall to the uniaxial compressive strength of the surrounding rock. Diederichs et al (2010) have summarized in situ observations of the extent of spalling for circular tunnels in the plot reproduced in Figure 10. This plot shows that the spalling depth is controlled by the ratio of the maximum stress on the tunnel boundary to the uniaxial compressive strength (UCS) or the crack initiation stress (CI).

Progressive spalling in the AECL URL Mine-by test tunnel

A classic case of progressive spalling is in the Mine-by Test Tunnel in the Atomic Energy of Canada, Ltd. Underground Research Laboratory (URL) at Pinawa, Manitoba, Canada. The layout of the URL is shown in Figure 11. The final spall boundaries in this tunnel are illustrated in Figure 12. These spalls have been studied in detail by numerous authors including Martin et al (1996), Martin (1997), Diederichs et al (2004) and Diederichs (2007).

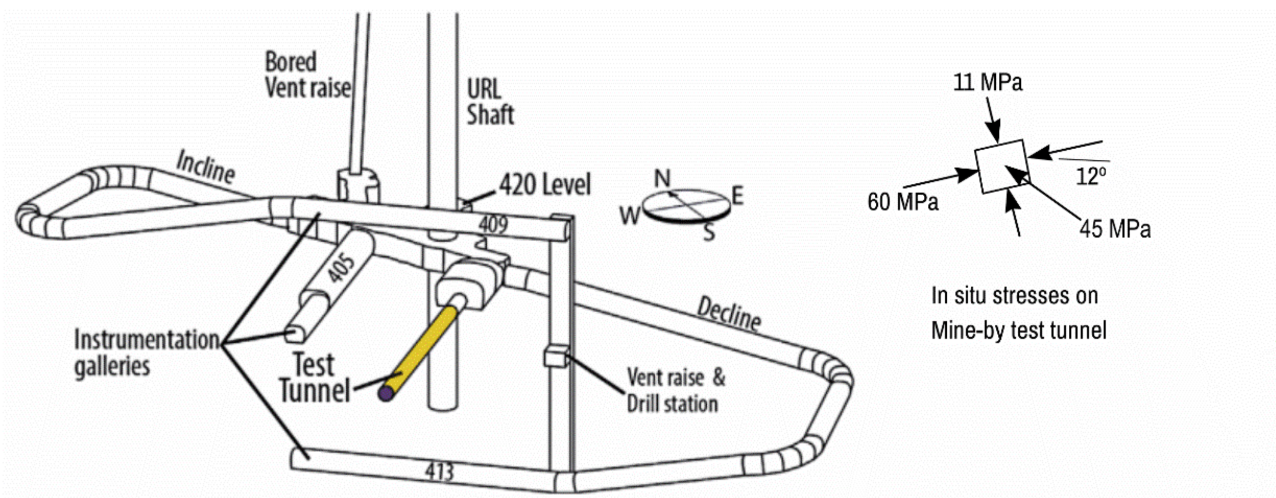

Figure 11: AECL URL Mine-by Test Tunnel excavated in Lac du Bonnet granite at a depth of 420 m below surface. Modified from Martin and Read (1996).

During the excavation of the URL Mine-by tunnel, instruments for monitoring acoustic emission (AE) and micro seismic (MS) events were installed in the rock mass surrounding the tunnel. Read and Martin (1996) describe the results of these measurements. One of their plots is reproduced in Figure 13, showing spalling in the roof and floor. Acoustic emissions were measured in the tensile stress zones in the tunnel sidewalls, but no identifiable tensile cracks were found in these regions. It was assumed that these acoustic emissions were due to the formation of numerous parallel tensile cracks, the apertures of which were too small to detect visually.

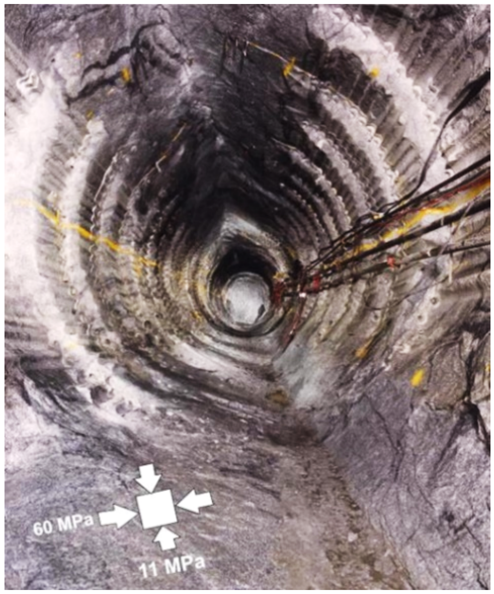

Figure 12: Spalling in the roof and floor of the Mine-by Test Tunnel. Note that the final roof and floor profiles shown here were only exposed after completion of the tunnel and excavation and scaling of the spalled material which remained attached to the boundary.

(Photograph provided by Professor C.D. Martin).

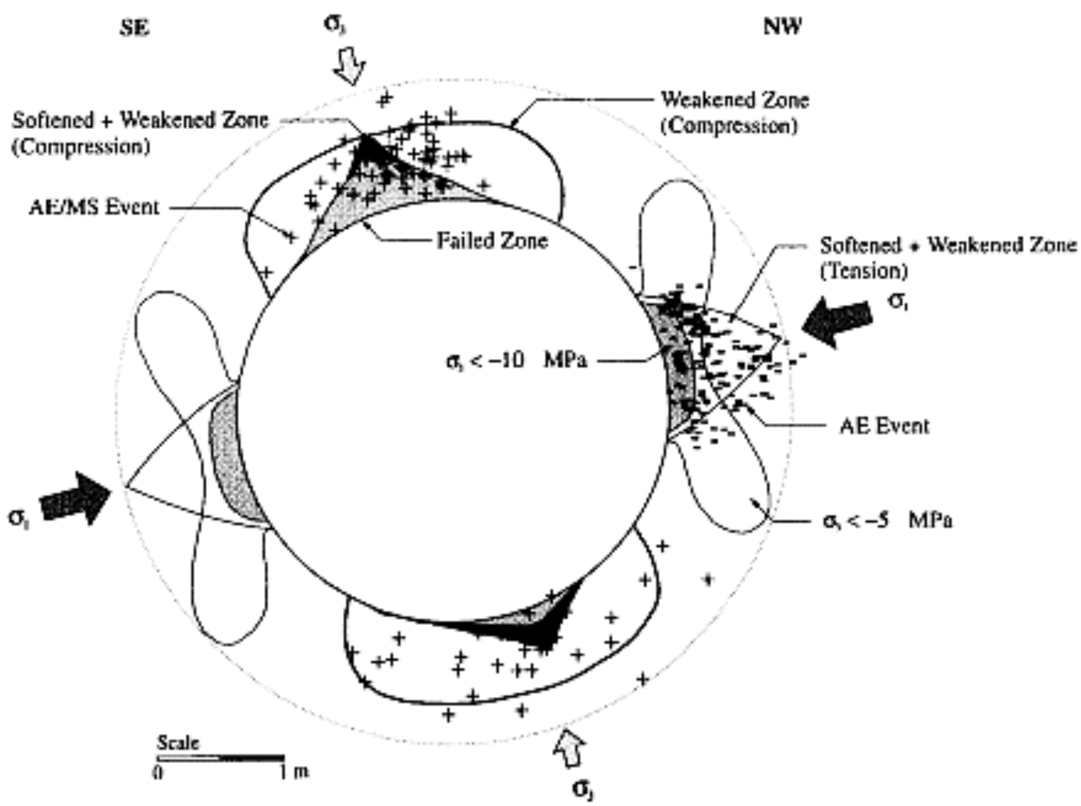

Figure 13: Excavation induced damage around the URL Mine-by tunnel. From Read and Martin (1996).

The URL was excavated in massive Lac du Bonnet granite, the mechanical properties of which were determined by Lau and Gorski (1992) in the CANMET laboratories in Ottawa, Ontario, Canada. The definition of the stresses at crack initiation, strain localization and peak strength plotted in Figure 14 are based on a modified figure from Martin and Christiansson (2009). Figure 15 shows the principal stress plots for crack initiation, onset of strain localization and peak strength for these tests.

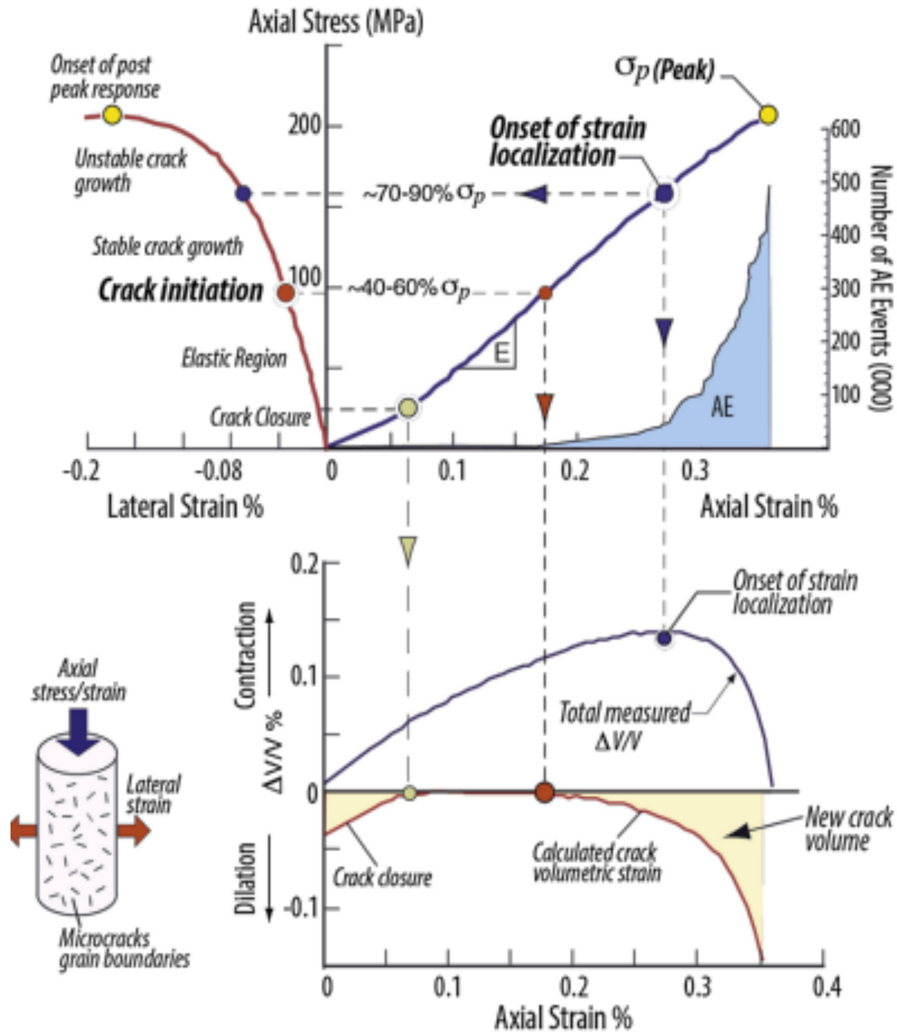

Figure 14: Stages in the progressive failure of intact specimens of Lac du Bonnet granite. Modified from Martin and Christiansson (2009).

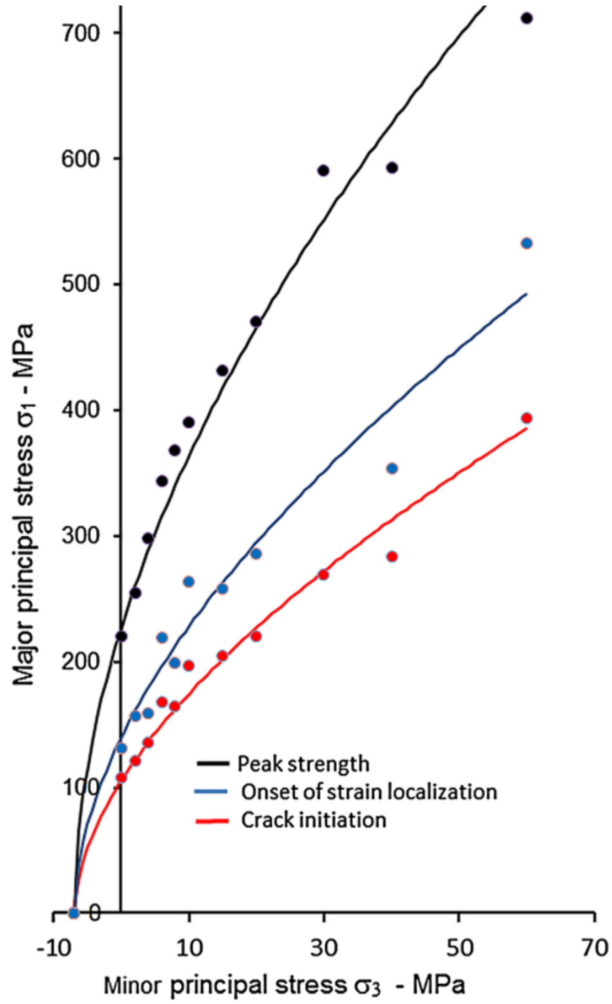

Figure 15: Tensile crack initiation, strain localization and peak strength for Lac du Bonnet granite from tests by Lau and Gorski (1992).

The transition from failure initiation to shear failure of the intact rock has been discussed extensively by Diederichs et al (2004), Diederichs (2007), Kaiser et al (2000), Kaiser (2006), Kaiser et al (2015), Bewick et al (2015) and Perras and Diederichs (2016). Several of these discussions have referred to research on the propagation of wing cracks from inclined Griffith cracks, summarized in Figure 9. The curves in Figure 9 show that the ratio of the length of the tensile wing cracks to the initiating defect, such as a grain boundary, decreases exponentially from a ratio of $\sigma_3/\sigma_1 = 0$ to almost zero at $\sigma_3/\sigma_1 > 0.1$. Note that some of these curves are based on the initiating defect being represented by an open elliptical crack (Hoek, Ashby and Hallam, Germanovich and Dyskin, Cai et al) while the curves published by Kemeny and Cook and by Martin are for closed sliding cracks, such as grain boundaries.

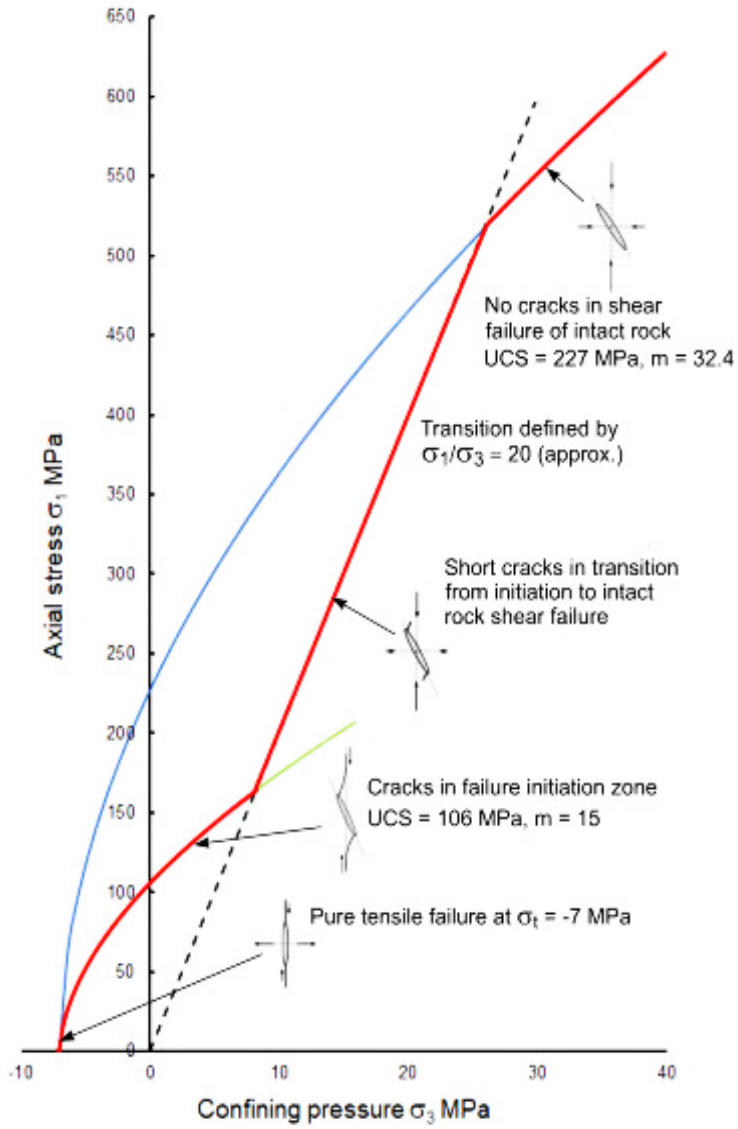

Figure 16: Composite failure curve for spalling of Lac du Bonnet Granite from Pinawa, Manitoba, Canada.

Figure 16 presents a composite failure curve, for intact and undamaged Lac du Bonnet granite, constructed using Hoek- Brown failure envelopes based on the triaxial test data shown in Figure 11. The envelope for fracture initiation is defined by the equation $\sigma_1 = \sigma_3 + CI\ (m.\sigma_3 + 1)$ ^0.5, with CI = 106 MPa and m = 15. The equation for the intact granite is $\sigma_1 = \sigma_3 + UCS\ (m.\sigma_3 + 1)$ ^0.5 where UCS = 227 MPa and m = 32.4. A uniaxial tensile strength $\sigma_t = -7$ MPa is based on direct tensile tests performed by Lau and Gorski (1992).

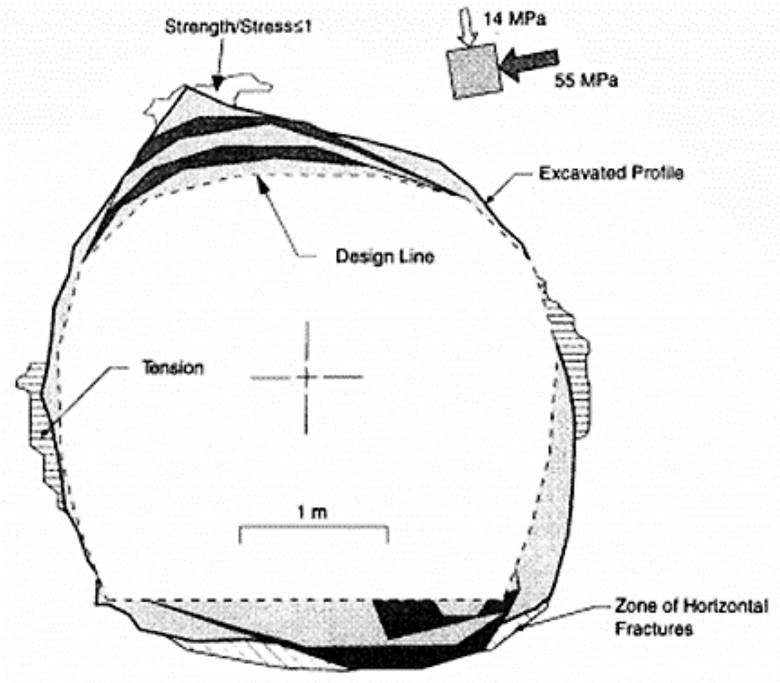

Figure 17: Numerical simulation of the slabbing process using elastic analyses and an elastic-brittle constitutive model. From Read and Martin (1996).

Observation of spalling in tunnels shows that this is a stepwise process in which each spall changes the boundary of the excavation and the surrounding stress field, resulting in the initiation of the next spall, as shown in Figure 17. The following quotation is from Martin (1997):

"In an attempt to simulate the slabbing process observed *in situ,* Read (1991) developed a routine within FLAC to conduct an iterative elastic analysis with explicit checks for tensile, compressive (shear) and slabbing failure based on a Hoek-Brown failure criterion with $\sigma_c = 100$, m = 12 and s = 1. A unidirectional tensile cutoff criterion was used in the case of tensile failure, which resulted in minor stress redistribution in the sidewalls of the tunnel. As in the previous analysis, compressive failure was noted close to the tunnel boundary in the roof and floor regions of the tunnel. Using a confining stress criterion in combination with a buckling criterion as a basis for removing elements at the free boundary, i.e., where the confinement was zero, Read (1991) found that the zone of removed material grew progressively, and was similar in shape to that observed *in situ.* He concluded that this type of modelling predicted responses for the instrumentation that were significantly different from those predicted by closed-form solutions for a circular hole in an infinite elastic medium. He also found that the shape of the predicted V-shaped notch was very dependent on the element removal scheme. Without the buckling constraint on the element removal scheme, Read (1991) found that the depth of the V-shaped notch approached *2a* where *a* is the radius of the tunnel.

However, with the buckling constraint, the depth of the V-shaped notch was reduced to *1.5a*."

At the time of Read's analysis in 1991, the concept of failure initiation at 45% of the uniaxial compressive strength of the intact rock had not been recognized. Hence, despite the promising results obtain by Read, his method was not adequate, and needs to be modified to incorporate the three-stage failure criterion shown in Figure 15. The step-by-step elastic analysis that I have carried out, using the RocScience finite element program RS2, is described below. Note that this analysis is for an idealized circular tunnel instead of the surveyed tunnel shape used by Read and Martin (1966).

Tensile failure in the tunnel sidewalls

As a tunnel is advanced through a stressed rock mass, the stresses on the tunnel boundary increase as the support provided by the rock mass ahead of the face decreases with distance from the face. The first boundary stress to exceed the available rock strength is in the tunnel sidewalls where the Strength Factor is 0.26 (σ_t = -7 MPa, σ_{min} = -27 MPa). No tensile cracks were observed in the tunnel sidewalls, so it was assumed that several parallel cracks, each with a very small aperture, occurred in the tensile stress zone. The propagation of these parallel tensile cracks is illustrated in Figure 18. The maximum depth of this cracked zone is 0.5 m, in the sidewalls of the 3.5 m diameter tunnel.

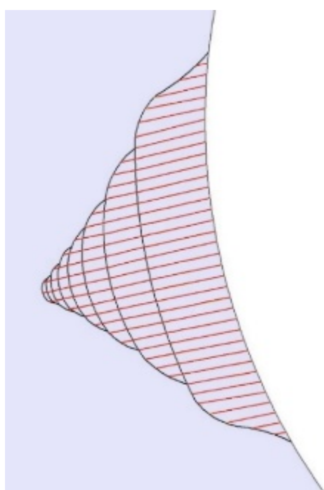

Figure 18: Progressive propagation of parallel tensile cracks in the sidewall of the Mine-by Tunnel.

Progressive spalling in the tunnel roof

The zone of potential failure initiation, defined by a Hoek-Brown failure curve with CI = 106 MPa and m = 15, is contained within the σ_1/σ_3 = 20 contours in Figure 16. Spalling failure can occur within this zone, with the spalls commencing at the tunnel boundary where the Strength Factor is 0.67 (CI/σ_{max} = 106/169), in the roof and floor. Typically, these initial spalls are about 3 cm thick plates, as illustrated in Figure 6.

As the spalls progress, it becomes increasing difficult for the failed material to fall away from the tunnel roof. In extreme situations, such as those illustrated in Figure 19, the spalls are confined and can only be dislodged by scaling using heavy mechanical equipment. The confined spalled material left in place, after the main spall has fallen away or been removed, is critical in defining the changed boundary shape used in the analysis of the next spall.

Figure 19: Confined spalls in the sharp corner of a square tunnel in a South African deep level gold mine. Depending on the changes in boundary shape, because of previous spalls, new spalls may find it difficult or impossible to escape from this confinement.

Photograph from the collection of Professor R.A.L. Black of the Royal School of Mines, Imperial College, London.

Read (1991) used a buckling criterion to estimate the constraint imposed on the slabs formed during the tunnel spalling process. I have experimented with numerous processes to investigate this constraint, including buckling of curved plates and Voronoi joint models, but while these studies have been very interesting, they did not produced results which were practical to implement in the modelling process discussed in this document.

The method finally adopted for the definition of the zone of spalled material that is free to fall is illustrated in Figure 20. This starts with the definition of the zone in which fracture can initiate, defined by the $\sigma_1/\sigma_3 = 20$ contours, as shown in Figures16. Within this zone, The Strength Factor contours are calculated, using the Hoek-Brown failure criterion with CI = 106 MPa and m = 15.

For $\sigma_1/\sigma_3 = 20$ and Strength Factors = 1.0 (light grey zone in Figure 20), fracture initiation can occur, but conditions for the development of spalling are not satisfied. Micro-seismic and acoustic emission events are likely to occur in this zone, as suggested in Figure 20.

For σ_1/σ_3 = 20 and Strength Factors < 1.0 (green zone in Figure 15), spalling can develop, but it is probable that some of this material will remain confined and will not be free to fall.

For Strength Factors < 0.93 (defined by the tangent point to the σ_1/σ_3 = 20 contour and shown as the red zone in Figure 20), the spalls are fully developed and free to fall from the roof of the excavation.

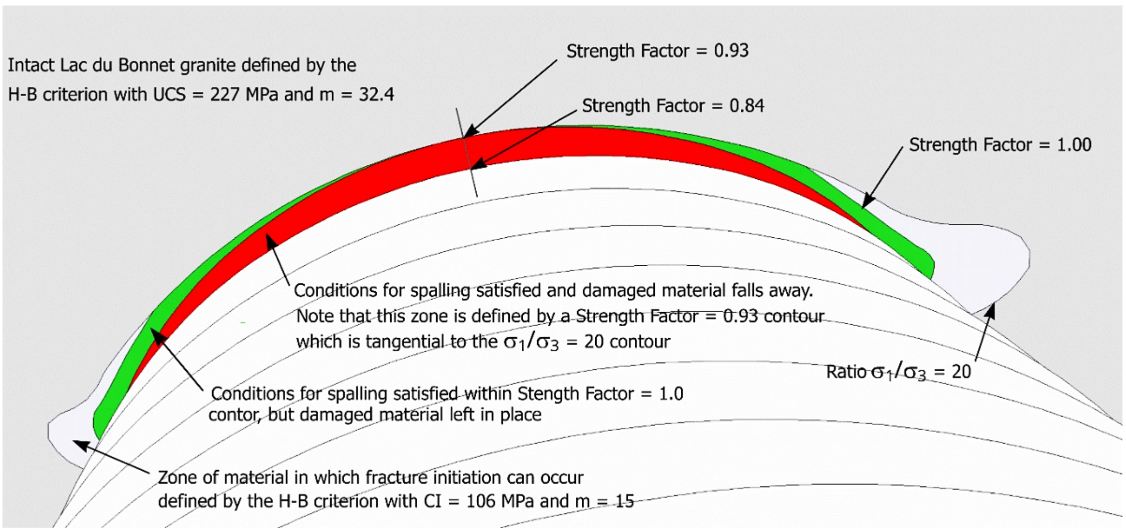

Figure 20: Definition of the 8th spalling zone in the roof of the Mine-by Tunnel.

Note that, in the floor of the tunnel, the first spall is identical to that in the roof, as shown in Figure 1. However, since this spall is generally covered by roadbed material and, as in the case of the Mine-by tunnel, it was only excavated after completion of the tunnel, the final shape of the floor spall zone is quite different from the roof spall.

The results of the complete spalling analysis for the roof of the Mine-by tunnel are presented in Figure 21, which includes the measured principal stress values at the peak of each of the 24 spalls. This analysis can be considered to produce an ideal collection of spalls in a completely homogeneous, isotropic intact rock. These conditions are seldom found in actual tunnels. It is interesting to compare the shape and depth of the 24th spall in Figure 21 with the surveyed shapes of the actual spalls in the Mine-by tunnel, shown in Figure 22.

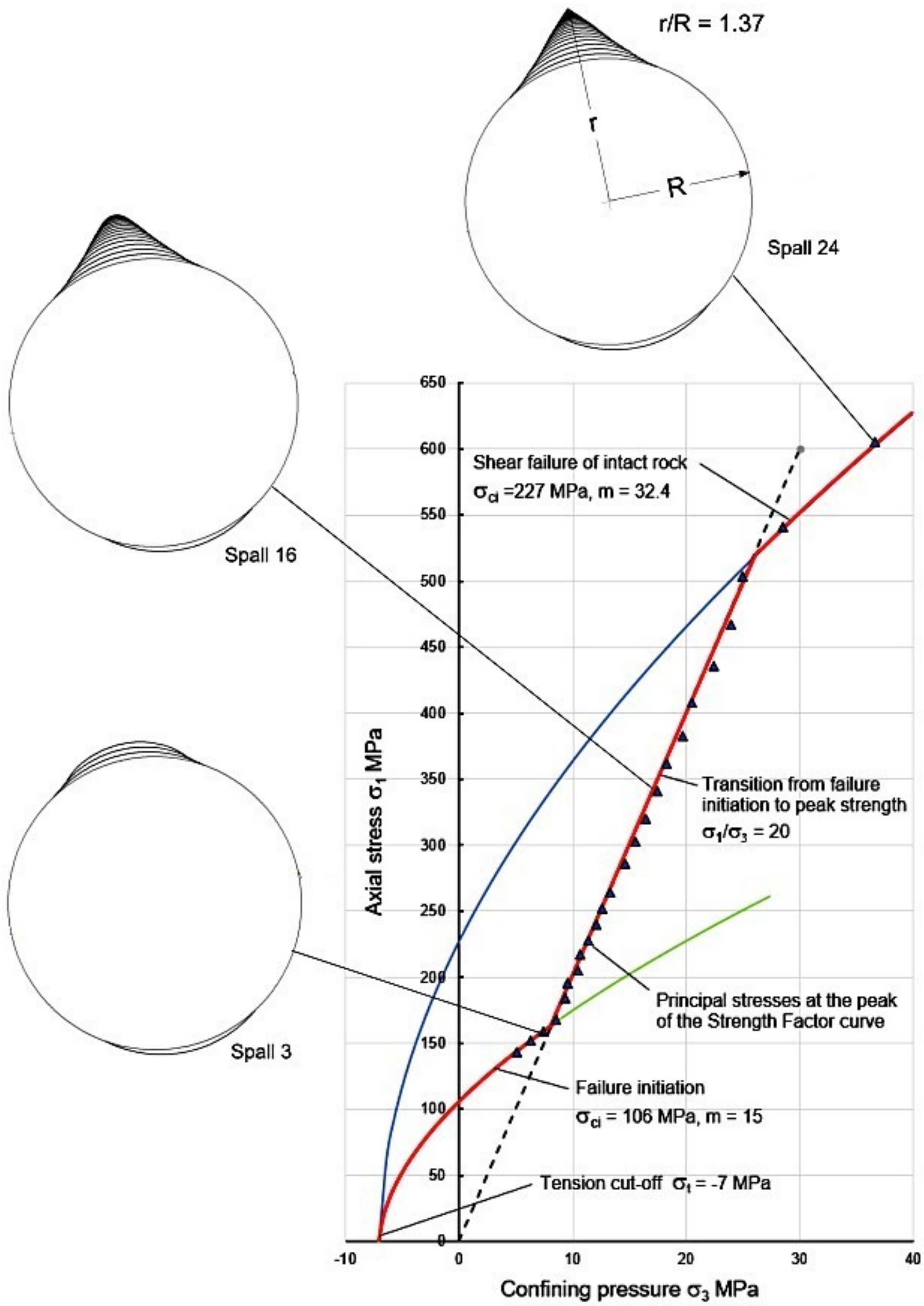

Figure 21: Composite failure curve for spalling of Lac du Bonnet Granite in the URL Mine-by Tunnel, with predicted spalls and maximum stress values for each spall.

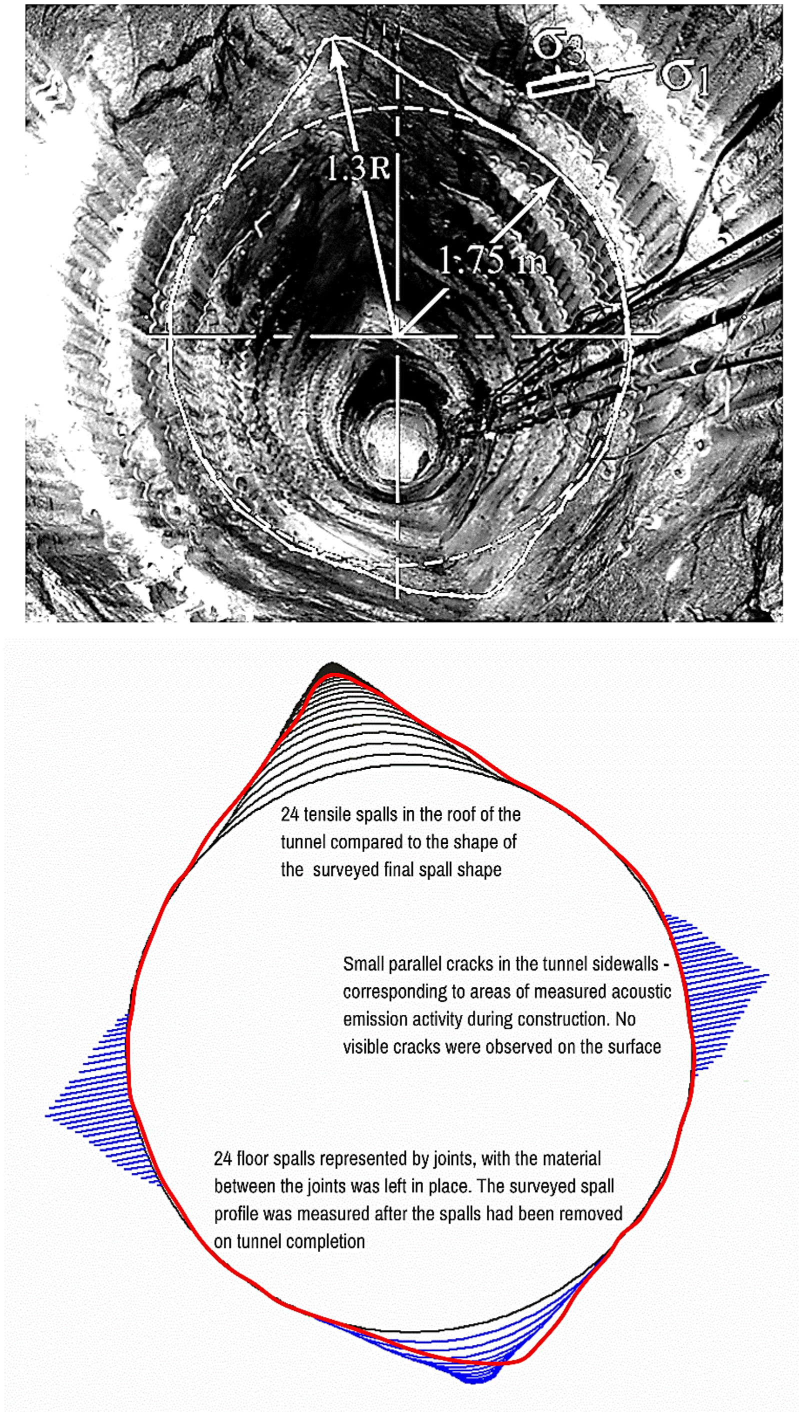

Figure 22: Comparison between surveyed (red) and predicted spalls in the URL Mine-by Tunnel.

The value of this analysis lies not in its absolute accuracy, but rather in the fact that it follows a simple logical process that can be applied to any situation in which spalling can occur in brittle materials such as rock and concrete.

A major limitation of the analysis presented in this document is that it was performed using the Rocscience finite element program RS2 which requires information to be transferred between the modeler and the interpreter for each spall. While this is analysis provides a wealth of interesting and useful information, it is extremely time-consuming and, therefore, of limited use as a practical engineering design tool. However, if this analysis could be performed in a program, such as a boundary element program, which included both calculation and interpretation on the same screen, the usefulness would be considerably enhanced.

Tensile failure and progressive spalling in a model

Hoek (1965) investigated tensile failure and progressive spalling in rock plate models cut from blocks of a very uniform fine-grained Granite Aplite. This rock was known to be a potential source of severe rockbursting in very deep level mines and this was a main reason for its choice as a test material. Triaxial tests on 25 mm diameter core specimens of this rock were carried in the rock mechanics laboratory in the South African Council for Scientific and Industrial Research (CSIR) and in the laboratory operated by Professor W.F. Brace in the Department of Earth and Planetary Science at the Massachusetts Institute of Technology (MIT) in the USA. The results of these tests, summarized in Figure 23, show that the rock has a uniaxial compressive strength of σ_{ci} = 600.4 MPa, a Hoek-Brown constant m_i = 18.8 and a tensile strength σ_t = -22.2 MPa.

Before moving on to a discussion on spalling failures, tensile failures, which tend to develop in excavation boundaries at a much lower stress level, will be discussed. This question was studied on physical models with both glass and rock as the model materials as shown in Figures 24. The equipment used to carry out these studies is discussed in the Appendix 1.

The results of these studies are summarized in Figure 23. These cracks can only initiate at ratios of lateral to vertical stress (k) of less than 0.33 and the length of the cracks increases rapidly for $k < 0.1$. The main conclusion from these studies was that the development and propagation of a tensile crack has a negligible influence upon the initiation and propagation of spalling in the excavation boundaries at 90° to the tensile cracks. Consequently, in the following study of spalling, tensile cracks have been inserted into the numerical model to coincide with the length of the observed cracks in the rock plate model and, thereafter, the influence of the tensile cracks has been ignored.

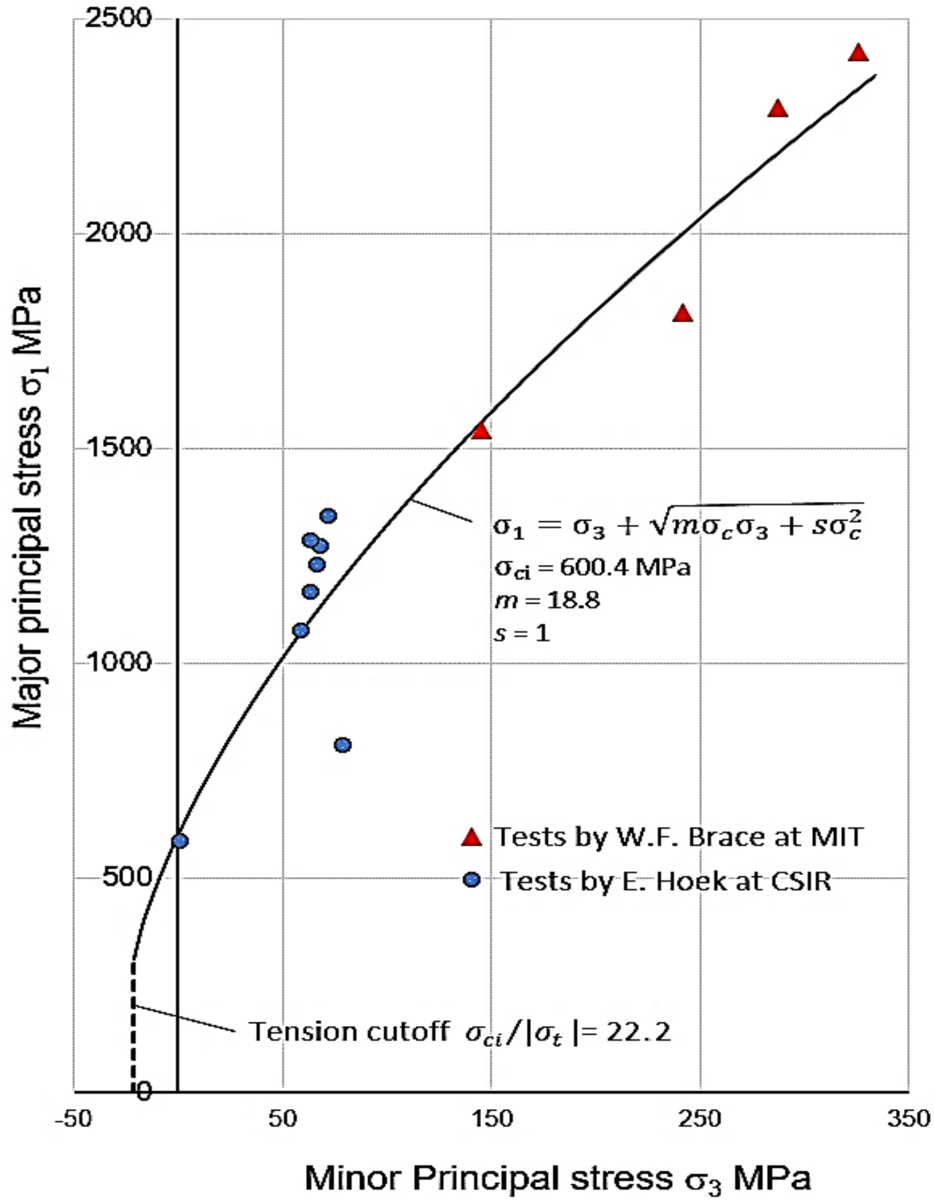

Figure 23: Results of triaxial tests on Granite Aplite. (After Hoek and Brown, 2018).

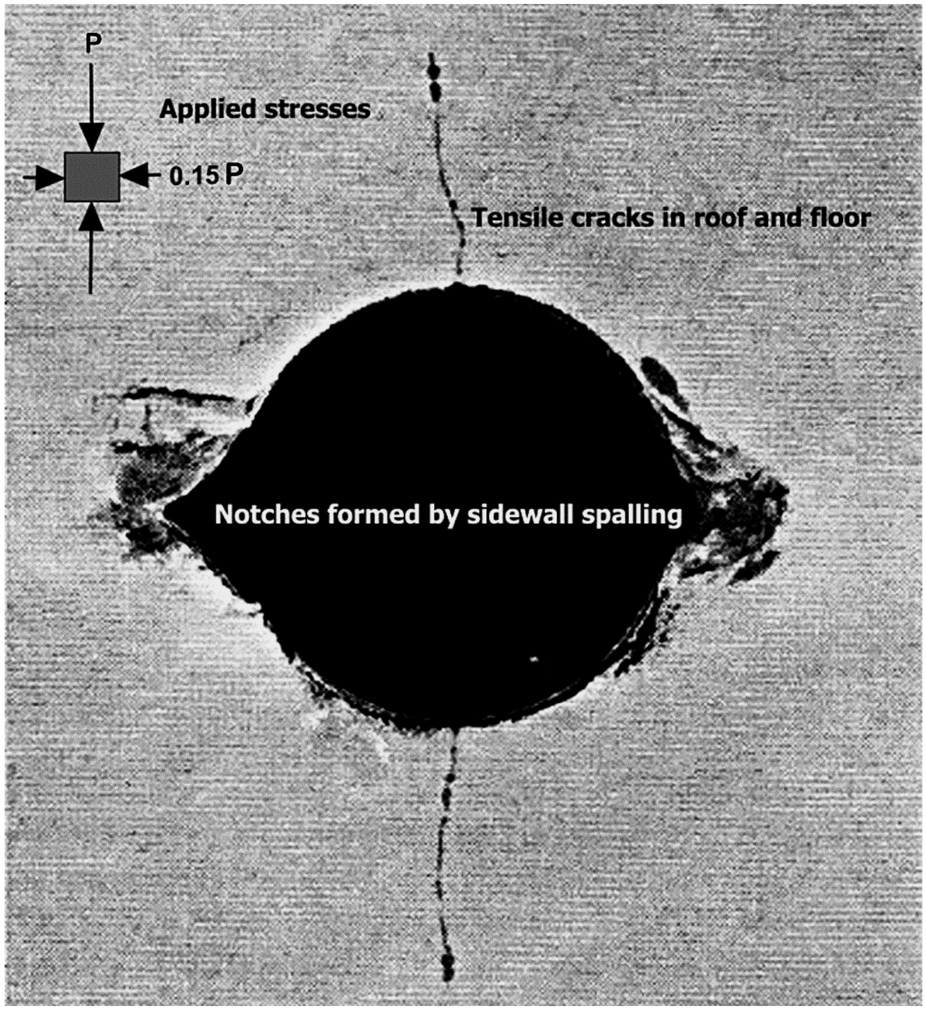

Figure 24: Development of tensile cracks in the roof and floor and spalling in the sidewalls of a 2.54 cm diameter hole in the rock plate model. Because of the lack of confinement normal to the faces of the model, some spalling occurred in the plane of the model. Despite this, the spall profile is clearly defined in the left-hand sidewall.

Initiation and propagation of spalling

No tests on fracture initiation were carried out on the Granite Aplite core in 1963 and hence, to construct a composite failure curve, it has been assumed that fracture initiation occurred at CI = 0.45 x σ_{ci} = 270.2 MPa. The tensile strength σ_t = -22 MPa is assumed to remain unaltered and the Hoek-Brown constant mi = 15 is estimated based on the Lac du Bonnet example. The transition from spalling initiation to intact rock failure has been assumed to occur at σ_1/σ_3 = 20. The resulting composite curve is shown in Figure 25.

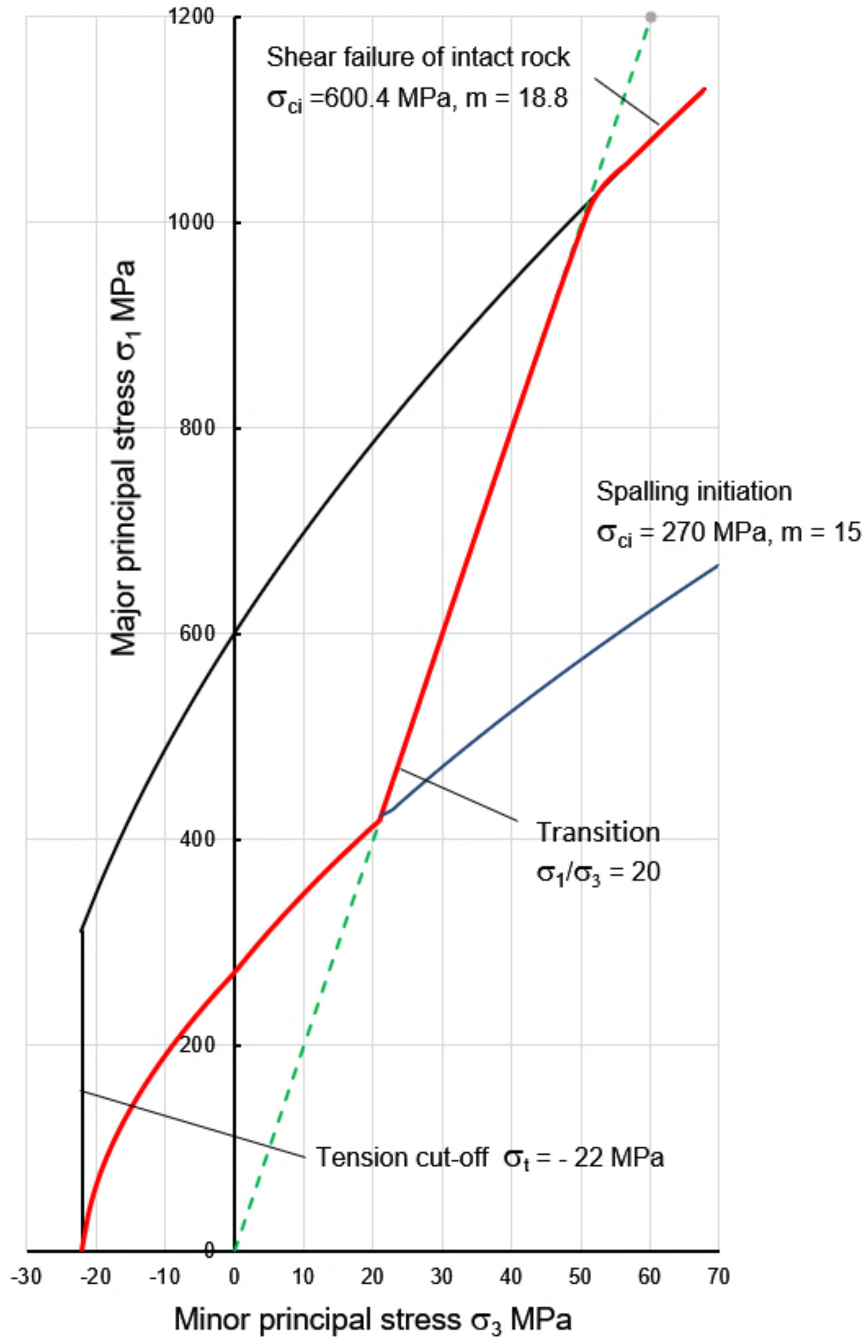

Figure 25: Composite failure curve for spalling of Granite Aplite.

Tensile cracks, in the roof and floor of the hole, initiated at an applied vertical stress of P = 61.5 MPa. This gives a tangential stress of $\sigma_\theta = P(3k - 1) = -33.8$ MPa. This is significantly higher than the -22.2 MPa given in Figure 23 and the difference is attributed to the epoxy resin photoelastic layer bonded to the model surface.

Based on the interpretation plotted in Figure 25, spalling in the excavation sidewalls can be expected to initiate at an applied vertical stress of $\sigma_v = 270.2 / (3 - k) = 95.4$ MPa. Unfortunately, in the photographic records available to me, it is impossible to detect this spalling initiation. The only reliable information is that reproduced in Figure 24 which shows that the sidewall spall is complete at an applied vertical stress of P = 175 MPa and a lateral stress of Q = 26.3 MPa. These stresses have been used in the following numerical analysis, recalling that spalling initiation would have occurred at a much lower stress level.

In the study of tensile failure and spalling, shown in Figure 24, a 15.2 cm square by 0.63 cm thick rock plate model was subjected to gradual increments of uniformly distributed vertical and lateral stresses in the equipment described in Appendix 1. A constant ratio of lateral and vertical stresses of k = 0.15 was used throughout the test.

Analysis of progressive spalling

A numerical model, representing the physical model illustrated in Figure 24, was constructed in the Rocscience program RS2 and used to model the sequential spalling sequence.

Definition of the conditions for spalling are shown in Figure 25. For low stress conditions, spalling can initiate when the ratio of the induced principal stresses σ_1/σ_3 exceed the Strength Factor defined by the Hoek-Brown criterion with CI = 270 MPa and mi = 15. As the levels of the induced principal stresses increase, the transition defined by the ratio $\sigma_3/\sigma_1 = 0.05$, is reached and the extent of spalling is limited by this line. At even higher stress levels, the transition curve will encounter the intact rock strength curve, defined by the Hoek-Brown criterion with UCS = 600.4 MPa and mi = 18.8, and spalling will occur in the intact rock.

Figure 26 shows the zone in which conditions for spalling are satisfied for the first spall in the RS2 model. This zone encompasses damaged material that can fall away as a spall and damaged material that remains is held in place by the geometry of the ends of the potential spall zone.

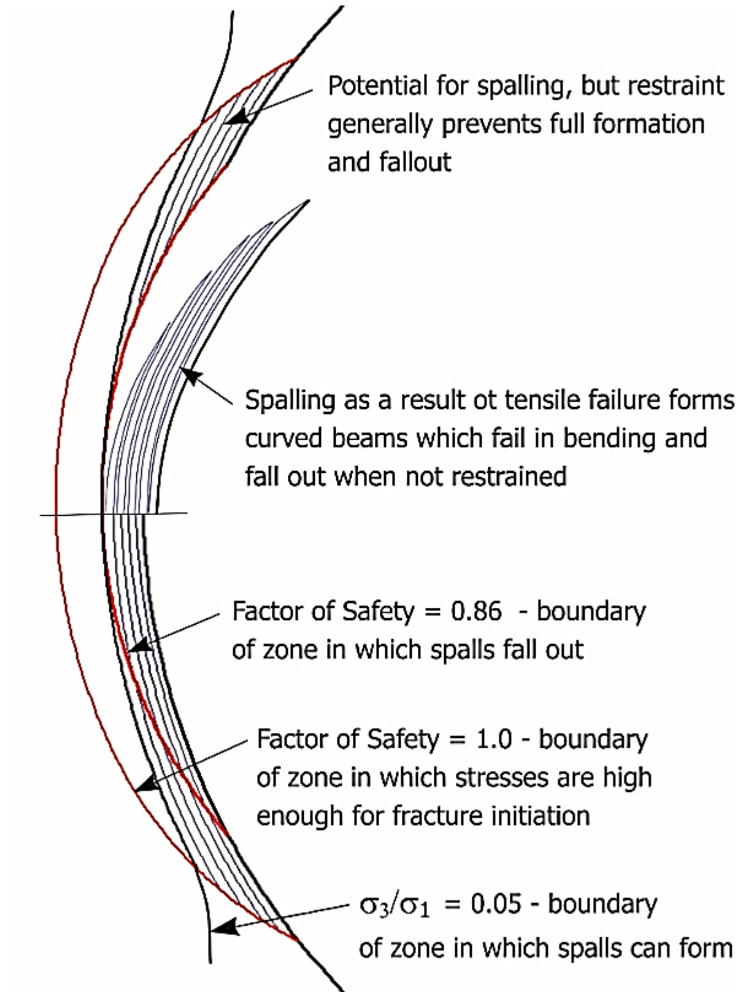

Figure 26: Definition of conditions for spalling and of the spall that falls away from the excavation sidewalls.

The successive spalls illustrated in Figure 26 were calculated by running 30 models in which the new geometry, created by removing the spall in each model, was the starting point for the next model. This proved to be a very robust procedure in which errors made in entering a spall were generally corrected by the following spall.

In developing this procedure, the major issue was to differentiate between damaged material that could fall away as a spall and damaged material that would be left in place. The final choice, defined in Figure 26, was based on my observations in many underground excavations, in which spalling was encountered, as well as numerical experiments in which details of the spalling process were simulated in numerical models.

Figure 27 shows excellent agreement between the predicted and measured spall profiles for this example.

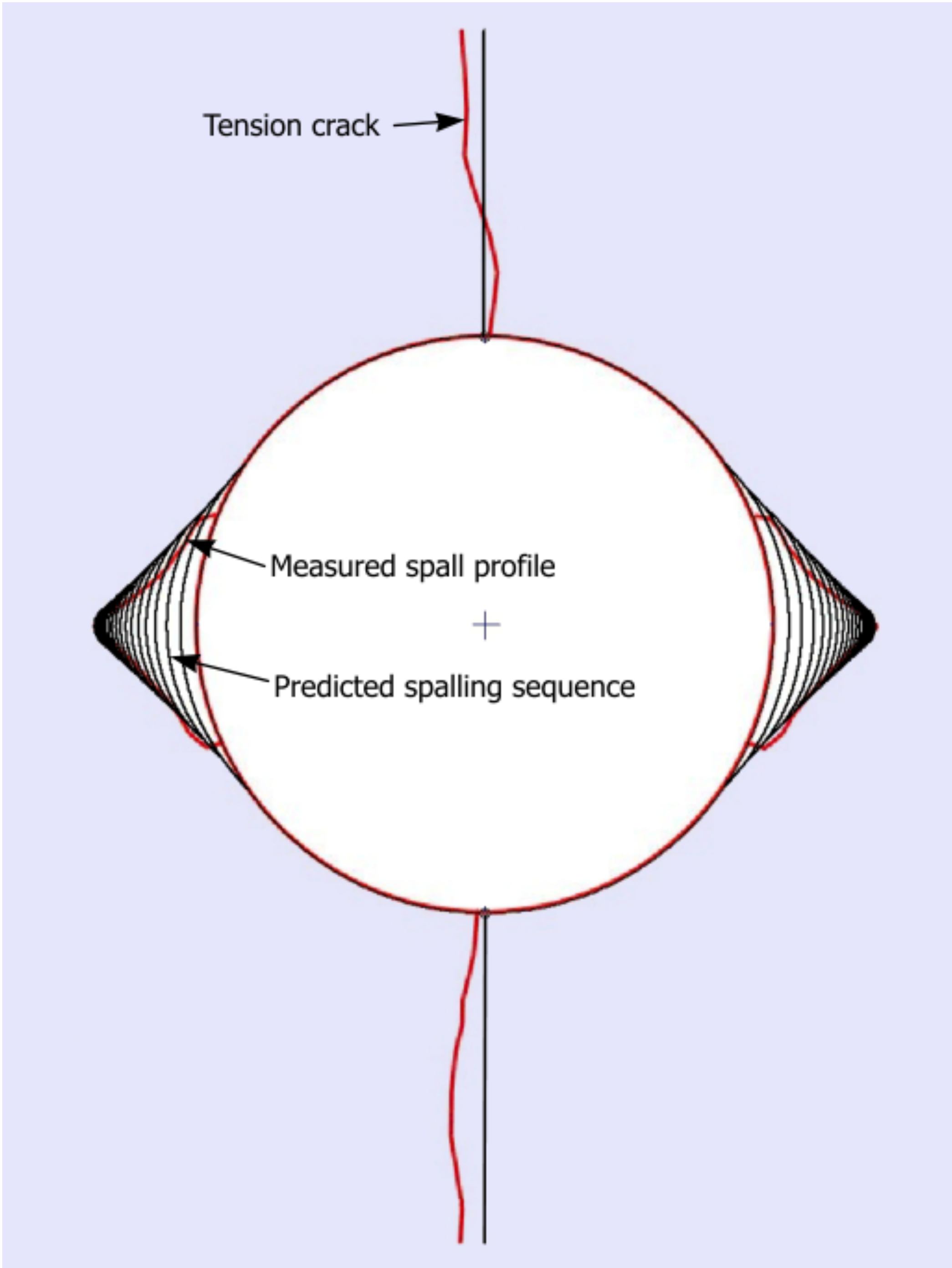

Figure 27: Comparison between predicted spalling sequence and profile and the measured profile in the model illustrated in Figure 22.

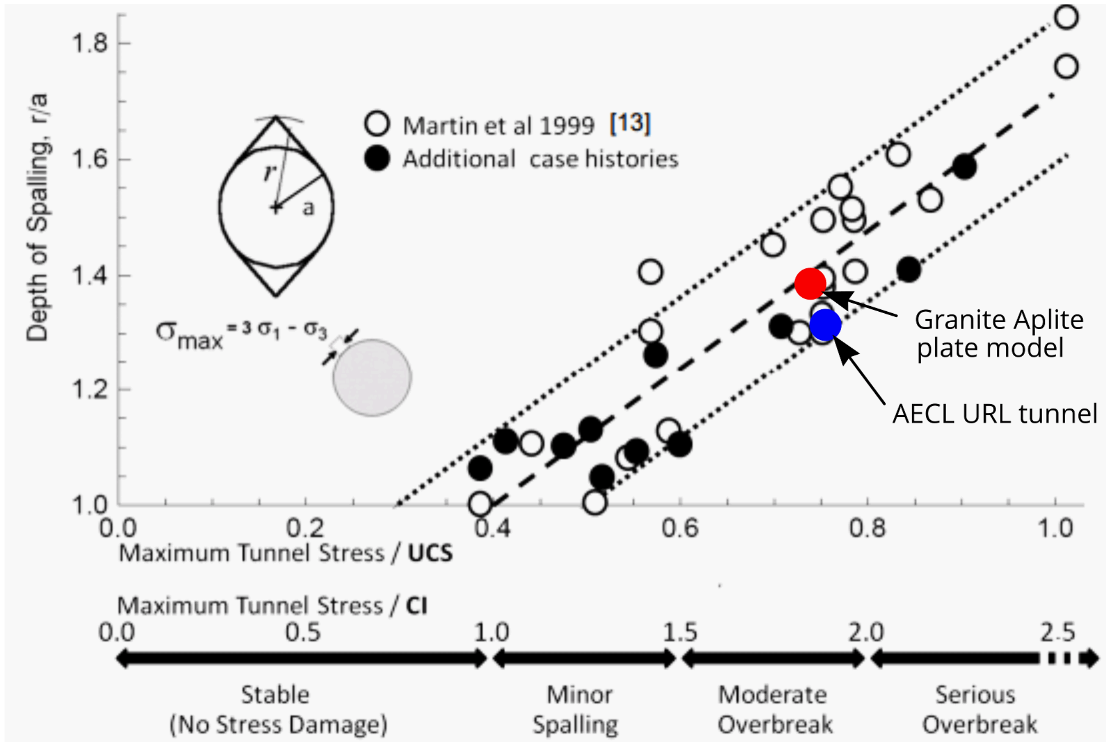

Figure 28: Plot of Figure 10 including AECL URL tunnel and Granite Aplite plate model results.

Progression from spalling into shear failure

In discussing the progression from tensile to shear failure in some circumstances, Shen and Barton (2018) offer the following comments:

> "We believe that tunnel spalling is a result of tensile fracturing due to excessive extensional strain caused by the uniaxial/biaxial compression stress state as the tunnel wall is approached. Tensile fracturing and spalling may be the start of a failure process at the early stage, but it is unlikely to be the root cause of massive failure. Further away from the wall/roof of an underground excavation, the confining stress (σ3) will be higher, and the major principal stress will be lower due to the moderation of stress concentration with distance from the opening. Hence, tensile fracturing conditions may not be met anymore. In this region, shear fracturing driven by high shear stress will be dominant. In other words, massive shear failures, not tensile failures, are needed to explain the observations at higher stress levels."

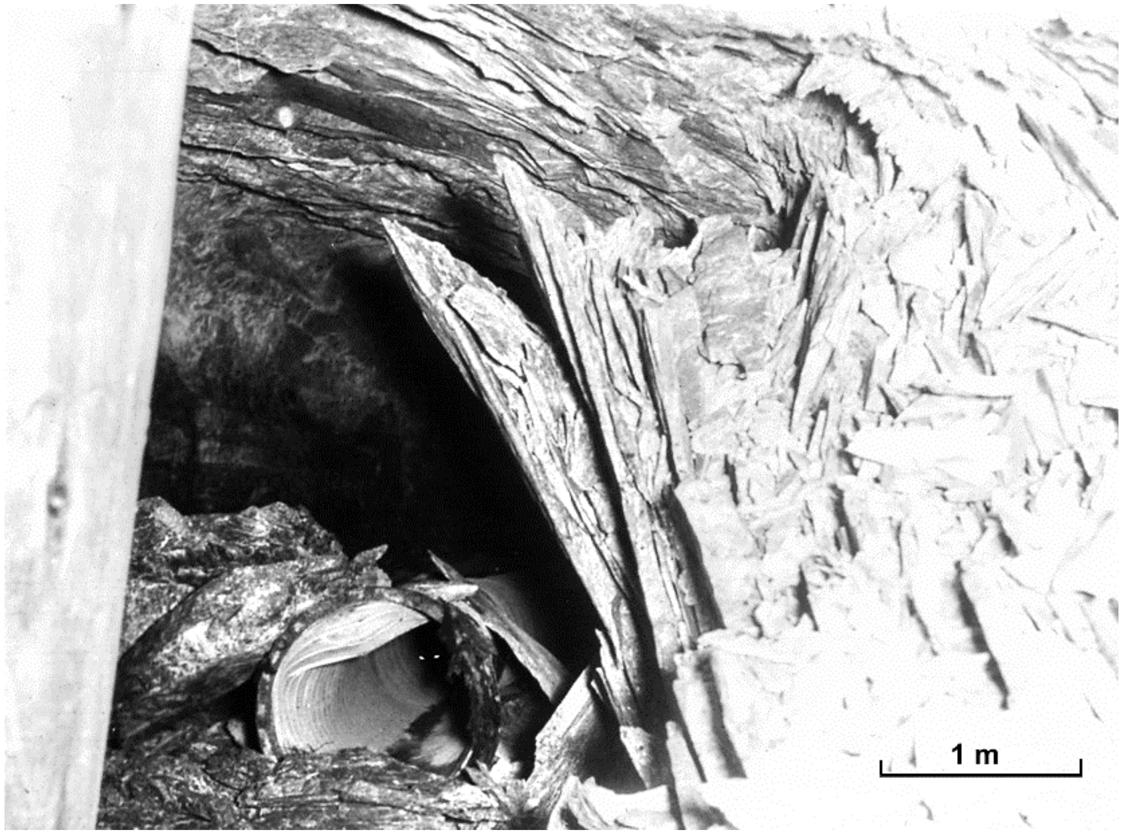

Figure 29: Results of a rock burst in a South African gold mine at a depth of approximately 3000 m below surface. This photograph was taken in the early 1960s and was included in a collection belonging to Professor R.A.L. Black of the Royal School of Mines in London.

The photograph reproduced in Figure 29 shows the remnants of an underground mine excavation in South Africa after a major rock burst. These events are extremely dangerous and practically impossible to predict.

As shown in Figure 30, the rock plate model shown in Figure 24 was loaded to failure. I do not have detailed information on the spalling and shear failure beyond the load used for the analysis shown in Figure 24, but I do have the set of reflected light photoelastic photographs shown. These indicate the growth of cracks parallel to the major principal stress trajectories in the rock remote from the excavation boundary and the eventual failure of the surrounding rock.

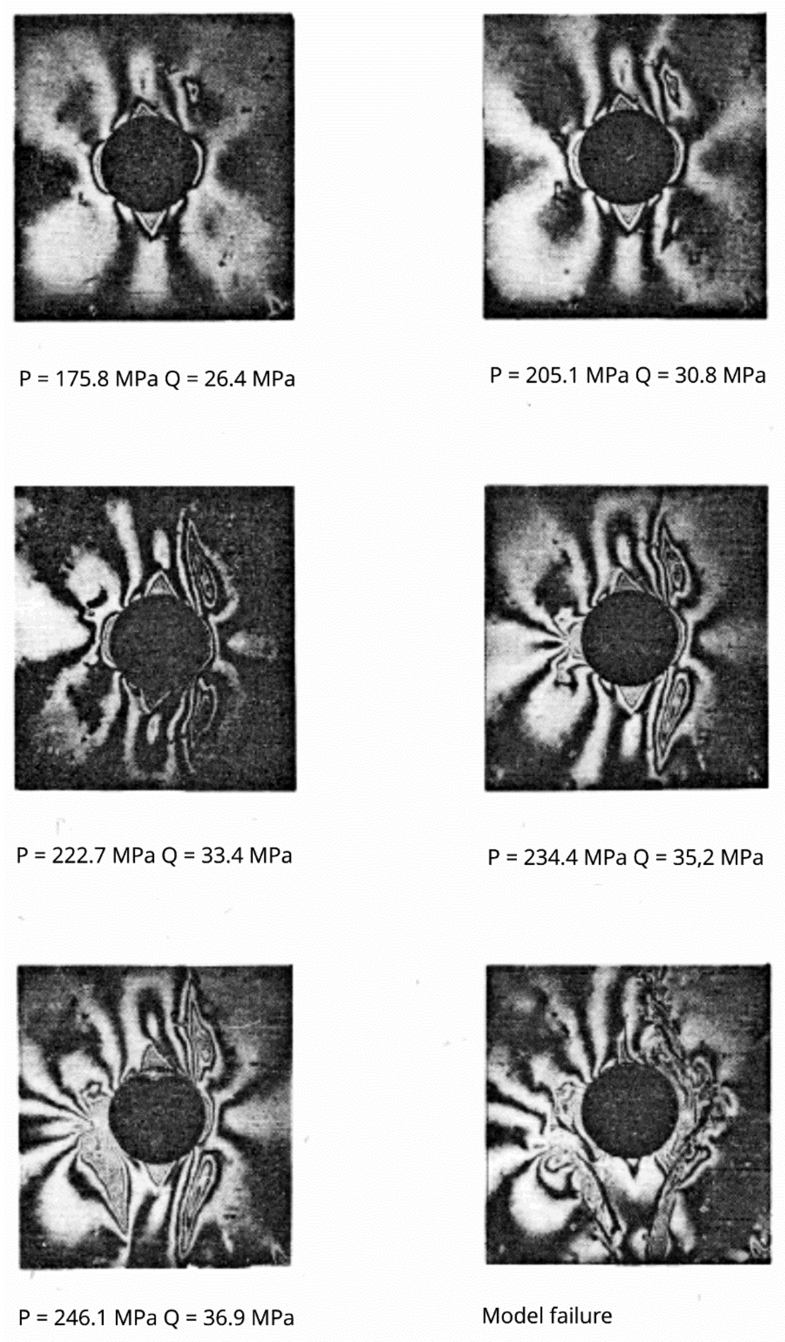

Figure 30: Reflected light photoelastic patterns captured by means of a high-speed flash unit during the loading to failure of a rock plate model. An epoxy resin layer had been bonded onto the rock surface by means of a reflective epoxy cement.

List of references

Ashby, M.F., Hallam. D. 1986. The failure of brittle solids containing small cracks under compressive stress. *Acta Metallurgica*. 34(3):497-510.

Bewick, R.P., Amman, F., Kaiser, P.K, and Martin. C.D. 2015. Interpretation of UCS test results for engineering design. *Proc. 13th International ISRM Congress*, Montreal.

Cai, M. and Kaiser, P, K. 2014. In-situ rock spalling strength near excavation boundaries. *Rock Mech. Rock Eng*., 47:659-675.

Cai, M., Kaiser, P, K, Martin, C.D. 1998. A tensile model for the interpretation of micro-seismic events near underground openings. *Pure and Applied Geophysics*. 153: 67-92.

Cain, S. and Diederichs, M.S. 2016. The impact of tunnel shape and profile details on brittle damage development. *Proc*. *Tunneling Association of Canada Annual Conference,* Ottawa, 2016.

Dyskin, A.V. and Germanovich, L.N. 1993. Model of crack growth in microcracked rock. *Int. J. Rock Mech. Min. Sci. and Geomech. Abstr.* 30(7):820.

Diederichs, M.S., Carter, T., Martin, C.D. 2010. Practical Rock Spall Prediction in Tunnel. *In Proceedings of World Tunneling Congress 2010* - Vancouver. 8 pages.

Diederichs, M. S. 2007. Mechanistic interpretation and practical application of damage and spalling prediction criteria for deep tunnelling. *Can. Geotech. J.,* 44, 1082-1116.

Diederichs, M.S., Kaiser, P.K. and Eberhardt, E. 2004. Damage initiation and propagation in hard rock tunnelling and the influence of near-face stress rotation. *International Journal of Rock Mechanics & Mining Sciences,* 41: 785-812.

Germanovich, J.N. and Dyskin, A.V. 1988. A model of brittle failure for material with cracks in uniaxial loading. *Mechanics of Solids* 23(2):111-112.

Hoek, E. 1965 Rock fracture under static stress conditions. Pretoria, *South Africa: Council for Scientific and Industrial Research Report MEG 383*. Also available at a PhD thesis from https://www.rocscience.com/learning/hoek-s-corner/publications.

Hoek, E. and Bieniawski, Z.T. 1965. Brittle rock fracture propagation in rock under compression. *International Journal of Fracture Mechanics*, 1,(3), 137-155.

Hoek, E. and Martin, D. 2014. Fracture initiation and propagation in intact rock – A review. *Journal of Rock Mechanics and Geotechnical Engineering*, 6,(4), 287–300.

Kaiser, P.K., Diederichs, M.S., Martin, C.D., Sharp, J. and Steiner, W. 2000. Underground works in hard rock tunnelling and mining. *GeoEng2000*, Technomic Publ. Co., 841-926.

Kaiser, P.K. 2006. Rock mechanics considerations for construction of deep tunnels in brittle rock. Keynote paper presented at the Asia Rock Mechanics Symposium in Singapore, 2006.

Kaiser, P.K., Bewick, R.P. and Amann, F. 2015. Overcoming challenges of rock mass characterization for underground construction in deep mines. *Proc. 13th International ISRM Congress*, Montreal.

Kemeny, J.M. and Cook, N.G.W. 1987. Crack models for the failure of rock under compression. In: Desai C,S, Krempl E, Kiousis P,D, Kundu T, editors. *Proceedings of the 2nd international conference constitutive laws for engineering materials, theory and applications*, vol. 1. London: Elsevier Science Publishing Co. 879-887.

Lau, J.S.O. and Gorski, B. 1992. Uniaxial and triaxial compression tests on URL rock samples from boreholes 207-045-GC3 and 209-069-PH3. *CANMET Divisional Report MRL 92 e 025 (TR)*; 1992. p. 46.

Martin, C.D. and Read, R.S. 1996. AECL's Mine-by experiment: a test tunnel in brittle rock. In: Aubertin M, Hassani F, Mitri H, editors. *Proceedings of the 2nd North American rock mechanics symposium*, Vol. 1. Rotterdam: A.A. Balkema; 1996. pp. 13-24.

Martin, C.D., Kaiser, P.K. and Alcott, J.M, 1996. Predicting the depth of stress-induced failure around underground openings. *In Proc. 49th Canadian Geotechnical Conference*, St. John's, C-CORE, Vol. 1, 105-114.

Martin, C.D. 1997. The 17th Canadian Geotechnical Colloquium: The effect of cohesion loss and stress path on brittle rock strength. *Canadian Geotechnical Journal*, 34 (5): 698-725.

Martin, C.D., Kaiser, P.K., and McCreath, D.R. 1999. Hoek-Brown parameters for predicting the depth of brittle failure around tunnels. Canadian Geotechnical Journal, 36 (1): 136-151.

Martin, C.D., Christiansson, R. 2009. Estimating the potential for spalling around a deep nuclear waste repository in crystalline rock. *International Journal of Rock Mechanics and Mining Sciences* 46(2): 219 -228.

Nicksiar, M. and Martin, C,D., 2013. Crack initiation stress in low porosity crystalline and sedimentary rocks. *Engineering Geology* 2013; 154: 64-76.

Ramsey, J. Chester, F. 2004. Hybrid fracture and the transition from extension fracture to shear fracture. N*ature* 2004.

Read, R.S. 1991. Mine-by Experiment - prediction of excavation-induced rock mass response. Technical Memorandum URL-EXP-022-M048, Atomic Energy of Canada Limited.

Read, R.S. and Martin, C.D. 1996. Technical Summary of AECL's Mine-by Experiment Phase 1: Excavation Response. AECL-11311, COG-95-171.

Perras, M.A. and Diederichs, M.S. 2016. Predicting excavation zone depths in brittle rocks. *Journal of Rock Mechanics and Geotechnical Engineering,* 2016, 60-74.

Shen, B. and Barton, N. 2018. Rock fracturing mechanisms around underground openings, *Geomechanics and Engineering*, Vol.16, No. 1, 2018, 35-47.

Stacey, T.S. 1981. A Simple Extension Strain Criterion for Fracture of Brittle Rock. Int. ,1. *Rock Mech. Min. Sci. & Geomech*. Abstr. Vol. 18. pp. 469-474.